Geophysical Research Letters

RESEARCH LETTER
10.1029/2019GL082116

Northern Hemisphere Land Monsoon Precipitation Increased by the Green Sahara During Middle Holocene

Weiyi Sun[1], Bin Wang[2], Qiong Zhang[3], Francesco S. R. Pausata[4], Deliang Chen[5], Guonian Lu[1], Mi Yan[1], Liang Ning[1], and Jian Liu[1,6,7]

[1]Key Laboratory for Virtual Geographic Environment, Ministry of Education, State Key Laboratory Cultivation Base of Geographical Environment Evolution of Jiangsu Province, Jiangsu Center for Collaborative Innovation in Geographical Information Resource Development and Application, School of Geography Science, Nanjing Normal University, Nanjing, China, [2]Department of Atmospheric Sciences and Atmosphere-Ocean Research Center, University of Hawai'i at Mānoa, Honolulu, HI, USA, [3]Department of Physical Geography and Bolin Centre for Climate Research, Stockholm University, Stockholm, Sweden, [4]Centre ESCER (Étude et la Simulation du Climat à l'Échelle Régionale) and GEOTOP (Research Center on the dynamics of the Earth System), Department of Earth and Atmospheric Sciences, University of Quebec in Montreal, Montreal, Canada, [5]Regional Climate Group, Department of Earth Sciences, University of Gothenburg, Gothenburg, Sweden, [6]Jiangsu Provincial Key Laboratory for Numerical Simulation of Large Scale Complex Systems, School of Mathematical Science, Nanjing Normal University, Nanjing, China, [7]Open Studio for the Simulation of Ocean-Climate-Isotope, Qingdao National Laboratory for Marine Science and Technology, Qingdao, China

Key Points:
- The first study of the impact of Saharan vegetation and dust reduction on the NHLMP
- Comparison with proxy records shows the effect of the Green Sahara improves the simulated NHLMP
- The Saharan vegetation and dust reduction significantly increase the NHLMP by 33.10%

Supporting Information:
- Supporting Information S1

Correspondence to:
J. Liu,
jliu@njnu.edu.cn

Citation:
Sun, W., Wang, B., Zhang, Q., Pausata, F. S. R., Chen, D., Lu, G., et al. (2019). Northern Hemisphere land monsoon precipitation increased by the Green Sahara during middle Holocene. *Geophysical Research Letters*, *46*. https://doi.org/10.1029/2019GL082116

Received 18 JAN 2019
Accepted 19 JUL 2019
Accepted article online 25 JUL 2019

Abstract Changes in land cover and dust emission may significantly influence the Northern Hemisphere land monsoon precipitation (NHLMP), but observations are too short to fully evaluate their impacts. The "Green Sahara" during the mid-Holocene (6,000 years BP) provides an opportunity to unravel these mechanisms. Here we show that during the mid-Holocene, most of the NHLMP changes revealed by proxy data are reproduced by the Earth System model results when the Saharan vegetation cover and dust reduction are taken into consideration. The simulated NHLMP significantly increases by 33.10% under the effect of the Green Sahara. The North African monsoon precipitation increases most significantly. Additionally, the Saharan vegetation (dust reduction under vegetated Sahara) alone remotely intensifies the Asian (North American) monsoon precipitation through large-scale atmospheric circulation changes. These findings imply that future variations in land cover and dust emissions may appreciably influence the NHLMP.

Plain Language Summary Northern Hemisphere land monsoon precipitation (NHLMP) provides water resources for about two thirds of the world's population, which is vital for infrastructure planning, disaster mitigation, food security, and economic development. Changes in land cover and dust emissions may significantly influence the NHLMP, but observations are too short to understand the mechanisms. The Sahara Desert was once covered by vegetation and dust emission was substantially reduced during the mid-Holocene (6,000 years BP), which provides an opportunity to test the models' capability and unravel these mechanisms. Here we use an Earth System model and find that when the Saharan vegetation and dust reduction are taken into consideration, the simulated annual mean precipitation over most of the NHLM regions shows a closer agreement with proxy records. The sensitivity experiments show that the North African monsoon precipitation increases most significantly under the regional effects of "Green Sahara." The Saharan vegetation (dust reduction under vegetated Sahara) alone also remotely increases the Asian (North American) monsoon precipitation through large-scale atmospheric circulation changes. The knowledge gained from this study is critical for improved understanding of the potential impacts of the land cover and dust changes on the projected future monsoon change.

1. Introduction

Understanding the dynamics of Northern Hemisphere land monsoon (NHLM) and reliably projecting its future changes are vitally important for infrastructure planning, disaster mitigation, food security, and water resource management (Wang et al., 2014; Wang et al., 2018). The changes in NHLM precipitation (NHLMP, defined in section 2.3) are driven by natural (Liu et al., 2013; Stevenson et al., 2017; Sun et al., 2017; Sun et al., 2019) and anthropogenic forcings (Devaraju et al., 2015; Dong et al., 2019; Giannini & Kaplan, 2018; Lau

et al., 2008; Vecchi et al., 2006) through the global sea surface temperature (SST) changes (Giannini et al., 2003) and are also affected by the low-frequency internal modes within the earth's climate system (Wang et al., 2013; Wang et al., 2017). Observations show that NHLMP intensified over the past three decades (Wang et al., 2012) due to both internal variability and the effects of climate change. Current climate models project an increasing trend in NHLMP over the 21st century (Lee & Wang, 2014). The increased Sahelian precipitation in the coming decades (Biasutti, 2013; Monerie et al., 2016) probably leads to an extension of Sahelian vegetation (i.e., grassland, shrubland, and wetlands) and reduced natural dust emission. However, human-induced overgrazing, deforestation and mismanagement of cropland can induce desertification, which might slow down the greening of Sahel (Engelstaedter et al., 2006; Evan et al., 2016). The vegetation and dust feedbacks are important not only for past and present monsoons but also for future monsoon changes (Wang et al., 2017). However, the impact of vegetation and dust on global climate has not drawn enough attention, and the processes by which these feedbacks change the climate have yet to be elucidated.

During the early to middle Holocene (11,000 to 5,000 years BP), increased summer insolation strengthened the African monsoon system. The Sahara Desert became once covered to a great extent by a mixture of shrubland, grassland, variable trees, and wetlands (Hély et al., 2014; Holmes, 2008), and the dust emissions were much lower than today (deMenocal et al., 2000; McGee et al., 2013), which led to the so-called "Green Sahara (GS)" or African Humid Period. Proxy data show that precipitation had increased substantially over the Saharan region during the mid-Holocene (MH, 6,000 years BP; Shanahan et al., 2015; Bartlein et al., 2011). Nevertheless, the simulations of the mid-Holocene performed in the Paleoclimate Modeling Intercomparison Project (PMIP), in which the land cover and dust concentrations are similar to that in the preindustrial period, fail to reproduce both the magnitude and the northward expansion of precipitation in North African (NAF) monsoon (Harrison et al., 2014). This is likely due to the fact that these models did not include the important feedbacks associated with changes in vegetation cover and dust concentrations (Pausata et al., 2016; Tierney et al., 2017). Moreover, in the context of the NHLM regions, the PMIP simulations not only underestimate the strength and extent of the NAF (i.e., Braconnot et al., 2012; Pausata et al., 2016) but also the Indian summer monsoon, East Asian monsoon, and North American monsoon (NAM; Braconnot et al., 2012; Zhao & Harrison, 2012; Bird et al., 2014). Some recent studies have indicated that the Green Sahara and dust reduction (GSRD) can have remote influences on the Arctic climate (Davies et al., 2015; Muschitiello et al., 2015), the El Niño–Southern Oscillation (Pausata, Zhang, et al., 2017) and tropical cyclones (Pausata, Emanuel, et al., 2017). In the present work, we use a series of sensitivity experiments with a fully coupled ocean-atmosphere model in which Saharan vegetation, dust concentration, and orbital forcing (ORB) are changed in turn in order to further investigate the role of vegetation and dust on NHLMP.

2. Data and Methods

2.1. Model Description and Experimental Design

The model used in this study is the version 3.1 of the climate model EC-Earth (Hazeleger et al., 2010). The atmospheric model is based on the Integrated Forecast System (cycle 36r4), including the H-TESSEL land model. The oceanic model is version 2 of the Nucleus for European Modeling of the Ocean (Madec, 2008), with a horizontal resolution of ~1° and 46 vertical levels. The model is also coupled with the Louvain-la-Neuve Sea Ice Model version 3 (Vancoppenolle et al., 2008). The coupling component is performed by the OASIS 3 coupler (Valcke, 2006). The preindustrial (PI) experiment is performed at T159 horizontal spectral resolution (1.125° × 1.125°, approximately 125 km) with 62 vertical levels, which is higher than the resolution in other PMIP models (Table S1 in the supporting information). The historical CMIP5 run from 1979 to 2008 based on EC-Earth (Present) is also conducted to represent the present-day climatology.

Based on the preindustrial condition, the first idealized sensitivity experiment (Green Sahara during preindustrial, PI_{GS}) is carried out (Table 1), which imposes the prescribed shrub vegetation type over the Saharan domain (11–33°N, 15°W–35°E). In our model, the surface albedo is decreased from 0.3 (for desert) to 0.15 (for evergreen shrub), and the leaf area index is increased from 0.2 (for desert) to 2.6 (for evergreen shrub). Pausata et al. (2016) tested the impact of replacing the evergreen shrub with grassland (albedo = 0.25) over eastern North Africa, showing no large impact on the strength of the western African monsoon. The test of NAF precipitation to these values in this study is also conducted in the supporting information (Figure S3), and the results are similar with Bonfils et al. (2001). The standard MH orbital forcing simulation (MH_{ORB}) is

Table 1
Description of the Model Experiments and Net Effect of Each Forcing

Simulation	Orbital forcing	GHGs	Saharan vegetation	Dust concentration
PI	1,850 AD	1,850 AD	Desert	PI
PI_{GS}	1,850 AD	1,850 AD	Shrub	PI
MH_{ORB}	6,000 year BP	6,000 year BP	Desert	PI
MH_{GS}	6,000 year BP	6,000 year BP	Shrub	PI
MH_{GSRD}	6,000 year BP	6,000 year BP	Shrub	Reduced

Abbreviation	Net effect of each forcing	Equation
ORB	Effect of orbital/GHGs forcing during the mid-Holocene	MH_{ORB}–PI
GS	Net effect of vegetation change during the mid-Holocene	MH_{GS}–MH_{ORB}
GS_{PI}	Net effect of vegetation change during the preindustrial	PI_{GS}–PI
GSRD	Combined effect of vegetation change and dust reduction during the mid-Holocene	MH_{GSRD}–MH_{ORB}

performed following the PMIP3 protocol (Braconnot et al., 2011), where the orbital value is set at 6,000 years BP. For the greenhouse gases (GHGs), methane is set at 760 ppb in PI and 650 ppb in MH_{ORB}, and there is no change in CO_2 and other greenhouse gases. The third experiment (MH_{GS}) imposes the prescribed shrub vegetation type over the Saharan domain, which is similar to the PI_{GS} experiment but under the MH orbital condition. We also perform the MH vegetated Sahara and reduced dust (MH_{GSRD}) experiment, where the Sahara land cover is also set to shrub but the dust concentrations are reduced by almost 80% in the troposphere over a broad area around the Sahara desert (Figure S1 in Pausata et al., 2016), according to the 60%–80% dust flux reduction from the proxy evidence (deMenocal et al., 2000; McGee et al., 2013). This imposed dust reduction results in a decrease in the local dust aerosol optical depth of approximately 60% and a decrease in the global total aerosol optical depth of 0.02. The initial conditions for each experiment are taken from a 700-year PI spin-up run, and the simulations are then run for 300–400 years. The quasiequilibrium is reached after 100–200 years, depending on the experiment. This research focuses on the last 100 years of each experiment.

For simplicity, we use ORB and GS to represent the net effect of orbital/GHGs forcing (MH_{ORB}–PI) and vegetation change (MH_{GS}–MH_{ORB}) during the MH, respectively (Table 1). The effect named GS_{PI} denotes the net effect of vegetation change under the PI condition (PI_{GS}–PI). GSRD is used to represent the combined effect of the vegetation change and dust reduction (MH_{GSRD}–MH_{ORB}) under the MH condition.

2.2. Observation and Proxy Data

The data set of the Global Precipitation Climatology Project version 2.3 (Adler et al., 2003), which provides global (land and ocean) coverage for the period of 1979–2017, was used to verify the model performance of the climatological pattern. The results of EC-Earth 3.1 are consistent with the observations in terms of land monsoon precipitation climatology compared to all of the PMIP3 models (Figure S1).

We also collected the precipitation proxy data to validate the simulated precipitation changes during the MH (about 6 ka BP; Table S2). The choice of proxy data needs to meet several criteria and these data are compiled from the published literature. First, the proxy data must reflect the precipitation or moisture conditions (precipitation minus evaporation). The records only reflecting temperature are not included. Second, the temporal resolution of proxies must be sufficient to reflect century-to-millennial scale climate changes. The MH proxy data are compared to the present day (0 ka BP).

2.3. Definitions of NHLM Area and Precipitation

Following the definition of global monsoon used by Wang and Ding (2008) and Liu et al. (2009), the NHLM area is defined by the land regions where the local summer mean minus winter mean precipitation exceeds 2 mm/day and the local summer precipitation exceeds 55% of the annual precipitation. Here summer is May– September, and winter is November–March. The NHLMP change is measured by the sum of summer precipitation anomalies in the NHLM area computed by each experiment (Hsu et al., 2012), which can better distinguish each forcing's effect on summer monsoon precipitation.

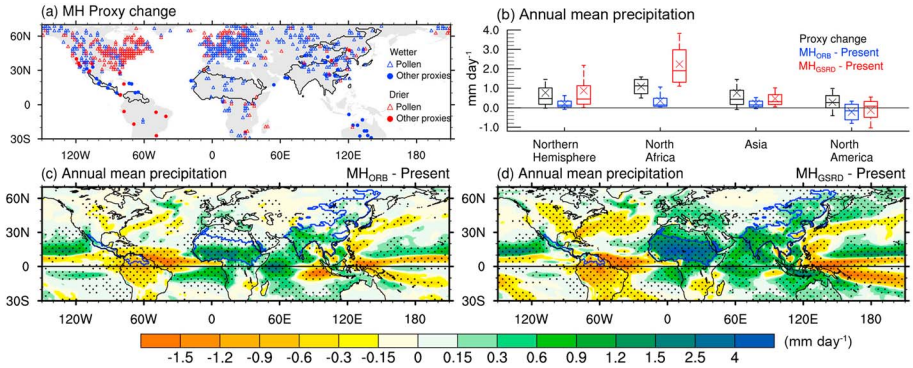

Figure 1. Annual mean precipitation change during the mid-Holocene. (a) Difference of the land precipitation between the mid-Holocene and present-day derived from the paleoclimate archives listed in Table S2. (b) Box-and-whisker plot of annual mean precipitation anomaly over NHLM regions from the pollen reconstructions (black), EC-Earth MH_{ORB} experiment (blue) and MH_{GSRD} experiment (red), relative to the present-day. The box whisker plots show the 10th, 25th, 50th, 75th, and 90th intervals, and the crosses denote the weighted regional mean precipitation change. (c and d) Annual mean precipitation anomalies (mm/day) in the MH_{ORB} and MH_{GSRD} experiments, respectively, relative to the present-day. Black lines in a, and blue lines in c and d represent the land monsoon regions defined by the MH_{GSRD} experiment. The dots denote areas in which the changes are significant at the 95% confidence level using a two-tailed Student's *t* test.

Due to the lack of proxy records that cover the entire monsoon domain (Figure 1), we use the weighted-area average annual mean precipitation over the same NHLM area to compare the proxy data and model results in Figure 1b. The NHLM area in Figure 1 is derived from the MH_{GSRD} experiment because it can better capture the expansion of NAF revealed by proxies during the MH (Pausata et al., 2016).

3. Results

3.1. Changes in the NHLMP

During the MH, most of the PMIP models simulate enhanced (reduced) Northern (Southern) Hemisphere monsoon precipitation due to the increased (decreased) summer insolation over the Northern (Southern) Hemisphere (Jiang et al., 2015; Zhao & Harrison, 2012). The MH_{ORB} experiment shows the very similar NHLM area and precipitation changes compared with the multimodel ensemble mean results in the PMIP3 (Figure S2).

The model results from the MH_{ORB} and MH_{GSRD} experiments are first compared with proxy data (Table S2) to check whether the simulated annual mean precipitation over the NHLM is improved under the imposed Saharan vegetation and dust reduction during the MH (Figure 1). When only the orbital/GHGs forcing (MH_{ORB}–Present) is considered during the MH, the NHLM annual mean precipitation change relative to the present-day is considerably underestimated (Figure 1b), which is similar to the ensemble mean results in PMIP3 (Braconnot et al., 2012).

When the Saharan vegetation and dust reduction (MH_{GSRD}–Present) are also considered, the annual mean precipitation change over most of the NHLM regions shows a closer agreement with proxy records (Figure 1b). The model overestimates the changes in NAF annual mean precipitation, compared to the proxy data. However, the simulated precipitation change shows a good agreement with proxy data between 15 and 30°N over the NAF, compared with that in the MH_{ORB} experiment (Figure S3a). Precipitation is mainly overestimated (3 mm/day) between 10 and 15°N, but recent proxy data suggest this increase could be plausible (Hély et al., 2014). The Asian monsoon (ASIA) precipitation is also enhanced, yielding a better agreement with the reconstructions (Figure 1b). Most of the proxy data indicate wetter conditions over the North American monsoon (NAM) for the Green Sahara period relative to current conditions (Figure 1a and Table S2), but the increased amplitude is smaller than that in the NAF and ASIA (Figure 1b). This increased annual mean precipitation over the NAM revealed by proxy data is still not reproduced under MH_{GSRD}–Present. In the areas outside the NHLM domain, the MH_{GSRD} experiment shows the increased precipitation over Europe and central Australia and the decreased precipitation over the central-eastern North America

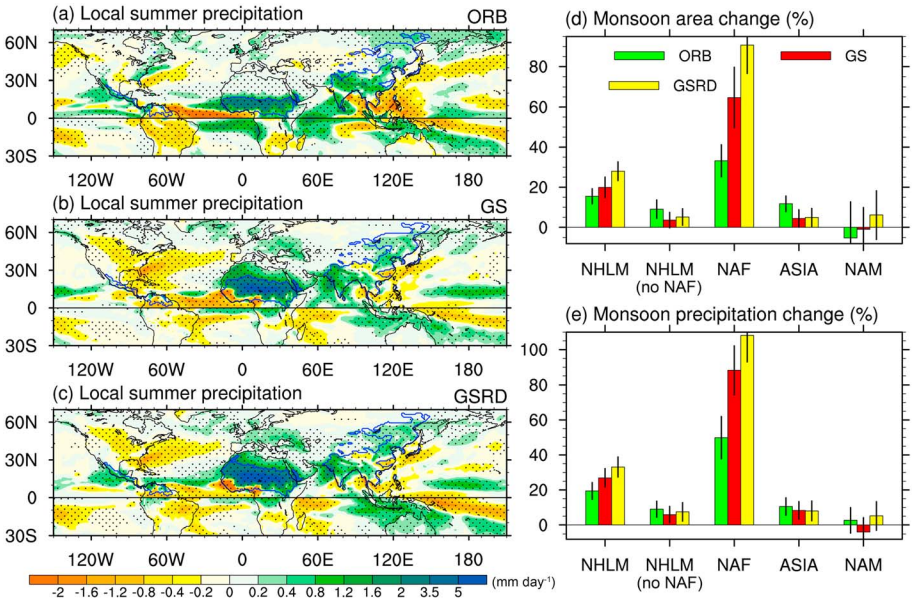

Figure 2. Land monsoon precipitation changes. (a–c) Local summer precipitation anomalies (mm/day) under ORB, GS, and GSRD, respectively. Local summer represents May to September in NH and November to March in SH. Blue lines in a–c highlight the land monsoon areas in the MH_{ORB}, MH_{GS}, and MH_{GSRD} experiments, respectively. The dots denote areas in which the changes are significant at the 95% confidence level via a two-tailed Student's *t* test. (d and e) Change rates (%) in land monsoon area and precipitation, respectively. Monsoon regions include NHLM, North African (NAF), Asian (ASIA), and North American (NAM) monsoon. "No NAF" denotes the area that does not include the North African monsoon. Green bars represent the results in ORB, red bars represent the results in GS, and yellow bars denote the results in GSRD. The black vertical lines over the bars show the range of one standard deviation.

and South America (Figure 1d), which is more consistent with the proxy data than that in the MH_{ORB} experiment.

To further quantify the NHLM changes, the NHLM area and NHLMP are analyzed. In GSRD, the NHLM area and precipitation are enhanced by 28.0% and 33.1%, respectively (Figures 2d and 2e), while under ORB, they are only enhanced by 15.5% and 19.4%, respectively; the increases are more than 1.7 times as large as that caused by the orbital/GHGs forcing. This is in better agreement with the proxy data (Braconnot et al., 2012; Figure 1b). Among the monsoon subregions, the northward expanded and enhanced North African monsoon contributes most to the NHLM area and precipitation changes under GSRD (Figures 2c–2e). Interestingly, in addition to its impact on local precipitation, GSRD also significantly enhances the precipitation over the NHLM (no NAF) by 7.5% (Figure 2e), especially for the Asian monsoon precipitation (8.0%); the increase in precipitation is significant and almost equal to that under ORB. Additionally, the North American monsoon precipitation is increased by 5.2% under GSRD, but this change is not significant due to large uncertainties (Figure 2e).

GS alone increases the NHLM area and precipitation by 19.9% and 26.9%, respectively, which means that the Saharan vegetation plays a greater role in strengthening the NHLM, compared with the dust reduction. The North African monsoon precipitation contributes most to the NHLM precipitation, followed by the significantly enhanced Asian monsoon precipitation (8.3%; Figure 2e). Suppressed precipitation is found over North America, but its amplitude is weak. We also use the GS_{PI} (Table 1) to isolate the individual effect of Saharan vegetation. The result shows that the NHLM area and precipitation are enhanced by 20.4% and 29.2%, respectively, which is almost equal to the effect of vegetated Saharan in the MH (Figures S4c and S4d). The distribution of precipitation anomalies over the monsoon subregions under GS_{PI} is also very similar to that under GS (Figures S4a and S4b). This means that the Saharan vegetation control the precipitation difference between MH_{GS} and MH_{ORB}, instead of the insolation or the nonlinear changes between vegetation and insolation. We also check the net effect of dust reduction under vegetated Sahara (GSRD–GS). The results show that it can further substantially enhance the North African monsoon precipitation by

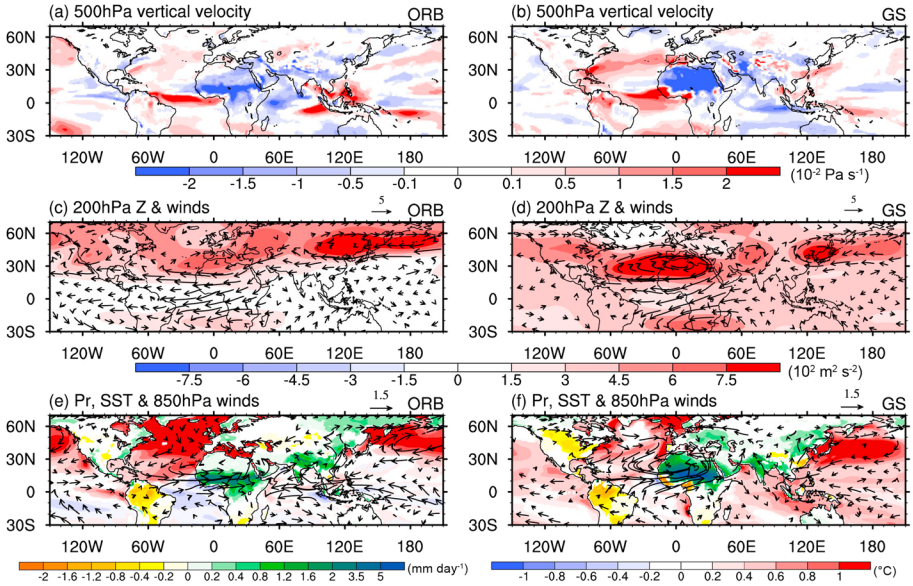

Figure 3. Northern Hemisphere atmospheric circulation changes during MJJAS. (a and b) Vertical velocity anomalies at 500 hPa (red shadings indicate descending motion while blue shadings denote ascending motion). (c and d) Geopotential height (shadings, 10^2 m^2/s^2) and wind anomalies (vectors, m/s) at 200 hPa. (e and f) Precipitation (shadings, mm/day), sea surface temperature (shadings, °C), and 850 hPa wind anomalies (vectors, m/s). Left panels represent the results in ORB, and the right panels denote the results in GS. Only the significant anomalies with confidence level exceeding the 95% (via a two-tailed Student's *t* test) are displayed.

19.9% and significantly increase the North American monsoon precipitation by 9.1% (larger than one standard deviation).

Therefore, the Saharan vegetation and dust reduction not only strengthen the North African monsoon during the MH but also remotely enhance the NHLM (no NAF), and the influence of the vegetated Sahara plays a stronger role here, compared with the dust reduction.

3.2. Mechanism of the Green Sahara's Influence on NHLMP

Some previous studies consider that NHLMP changes are caused by the orbital-induced large-scale meridional temperature gradient and the land-ocean thermal contrast during the MH (Jiang et al., 2015; Zhao & Harrison, 2012). In this study, the summer anomalous zonal mean meridional temperature gradient, land-sea thermal contrast, and land-sea level pressure gradient are weaker over the NH (no NAF) under GSRD, compared with that under ORB (Figure S5). However, a significant increase in the NHLM (no NAF) precipitation is found under GSRD (Figure 2d). Thus, it can be inferred that the vegetated Sahara and dust reduction affect the NHLM (no NAF) mainly through other mechanisms.

The surface albedo is reduced over the vegetated Sahara, leading to a warming in the months preceding the monsoon and favoring a strong convection after that (Pausata et al., 2016). A significant tropical North Atlantic SST warming enhances the north-south thermal gradients (Figure 3f), strengthening the southwesterly anomalies, further enhancing the Sahelian precipitation (i.e., Kamae et al., 2017; Monerie et al., 2019). The surface cooling occurs between 10 and 23°N (Figure S6), which is caused by the latent heat release and the increased cloud cover reflecting solar radiation (Pausata et al., 2016; Ramanathan et al., 1989). An albedo-induced warming over the northern Sahara develops throughout the summer, enhancing the northward expansion of the North African monsoon (Figure 3f). The substantial increased monsoon precipitation leads to a release of latent heat, warming the middle and upper troposphere (Figure S6). This increases the atmospheric thickness and the upper-level geopotential height, inducing an anomalous anticyclone in the upper troposphere (Figure 3d). Then a noticeable baroclinic structure is exhibited in the entrance of the westerly jet (Figure S7). However, ORB causes the weaker middle and upper troposphere warming over the North African region (Figure S6), which induces a much weaker anomalous anticyclone in the upper troposphere (Figure 3c), compared with that under GS.

GS also induces an intensification and westward extension of the Walker Circulation over the Pacific Ocean (Figure S8) through changes in equatorial Atlantic SSTs, which is explained by Pausata, Zhang, et al., 2017 The changes in the Walker Circulation enhance the low-level southeasterly anomalies over the northern Indo-Pacific Ocean (Figure 3f), which enhances the South Asian monsoon (i.e., Ning et al., 2017; Wang et al., 2015). This intensified Indian summer monsoon can excite the anomalous upper-level west-central Asian high (Ding & Wang, 2005). Subsequently, two baroclinic structures (with the stronger one in North Africa and the weaker one in west-central Asia) are formed (Figure S7), generating a Rossby wave train. This wave energy propagates downstream to regions along the waveguide, which induces the barotropic structure over the regions of East Asia, the North Pacific and North America, which resembles the circumglobal teleconnection (CGT) pattern (Ding & Wang, 2005). Nevertheless, in the case of ORB, these two baroclinic structures are much weaker in North Africa and west central Asia (Figure S7).

Under GS, a barotropic structure located over Japan induces an anomalous low-level divergence center (Figures 3d, 3f, and S9). Anomalous southerlies over the west of this divergence center enhance the northward transport of water vapor to northern China, causing the increased precipitation (Figure S9b). Anomalous easterlies over the North Pacific carry more moisture into Southern Asia, increasing precipitation there. This intensifies the Asian monsoon precipitation. Additionally, GS induces the anomalous surface warming over the west-central Asia and Northwest Pacific (Figure S6b). This is because the wave-induced anticyclonic anomalies suppress the cloud cover and increase the incoming solar radiation. These two warming centers are conducive to enhance the northward moisture transport to the South and East Asia. However, the suppressed precipitation is found along the East Asian subtropical front due to the local descending motion. Thus, the Saharan vegetation indirectly enhanced the Asian summer monsoon through the upper-level Rossby wave train and a westward extension of the Walker Circulation.

In North America, an anomalous upper-level anticyclone covers most of the midlatitude region and induces the low-level divergent winds under GS (Figures 3d and 3f). Moreover, the strong heating over North Africa excites the Gill-type Rossby wave pattern (Gill, 1980), which induces the descending motion over the equatorial Atlantic Ocean and tropical South America, suppressing precipitation there. It also causes the descending motion over central-east North America (Figure 3b), which is located to the west of the North African heat source. These two descending motions may contribute to the decreased precipitation over the Western Hemisphere, which is observed in the proxy data (Figure 1a) and causes the easterly anomalies over the eastern equatorial Pacific (Figure 3f), slightly weakening the North American monsoon.

To validate that this mechanism is caused only by the effect of Saharan vegetation and is not a direct response to insolation or a combined effect of vegetation change and orbital forcing, we verify the results under GS_{PI}. The result shows that GS_{PI} also induces the upper-level wave train (Figure S10). A barotropic structure located near Japan causes a very similar atmospheric circulation pattern over the Asian monsoon region, compared with the results under GS. Descending motions also occur over tropical South America and central-east North America, suppressing North American monsoon precipitation. This additional experiment highlights the important role of the Saharan vegetation in changing the NHLMP.

Previous studies have shown that the dust reduction strengthens the vegetation feedback on radiative forcing, which enhances the North African monsoon (Gaetani et al., 2017; Pausata et al., 2016), but the mechanism of its impact on the North American land monsoon is unclear. The reduced dust concentration happens over the area of roughly 100°W–60°E, 10°S–40°N (Figure S1 in Pausata et al., 2016), which increases the downward solar radiation and warms the tropical North Atlantic SST (Figure S11). This causes the east-west temperature gradient from the eastern tropical Pacific to the western Atlantic Ocean, inducing the anomalous westerlies over the northeastern tropical Pacific, enhancing the North American monsoon precipitation. At the same time, there is also a dust reduction of about 40%–50% over the North American region (Pausata et al., 2016), which strengthens the local moist convection.

4. Discussion and Conclusions

Previous model studies showed an obviously underestimated NHLMP changes compared with the reconstructions in the MH (Braconnot et al., 2012; Jiang et al., 2015; Zhao & Harrison, 2012). They focused on the insolation changes and ignored Saharan vegetation and dust concentrations. Here we show that the vegetated Sahara and dust reduction can modulate the atmospheric circulation and affect the NHLMP. It

should be noted that only the direct effect of dust reduction is considered in this model version, while the indirect aerosol effect (nucleation that results in the formation of more rain droplets) is not included. This may affect the results shown in this study as suggested by a recent study focusing on the indirect effect on the West African monsoon (Thompson et al., 2019).

In summary, our results show that the simulated annual mean precipitation change is significantly improved over most of the NHLM regions during the MH compared with the reconstructions when the vegetated Sahara and dust reduction are also taken into consideration. These forcings increase the NHLMP by 33.1%, which is more than 1.7 times the impact of the orbital/GHGs forcing. Among the monsoon subregions, the strengthened North African monsoon precipitation contributes most significantly, which is mainly caused by the increased moisture convergence under the effects of vegetation and dust reduction. The Saharan vegetation alone also leads to the increased Asian monsoon precipitation by 8.0% through the upper-level wave train and a westward extension of the Walker Circulation, while dust reduction under vegetated Sahara enhances the North American monsoon by 9.1% through the anomalous westerlies induced by the tropical North Atlantic warming. These results indicate the strong impact of the Green Sahara on the NHLMP during the MH. They also suggest this factor may have a significant influence on the NHLMP in the future, which is critical for the demands of infrastructure planning, disaster mitigation, agriculture, and water resource management.

Acknowledgments
We thank two anonymous reviewers and editor for their insightful comments. We thank the climate modelling groups (listed in Table S1) for producing and sharing their model outputs, GPCP for providing the Version 2.3 data set, and every paleoclimate researcher who provides the proxy records (listed in Table S2). This research is jointly supported by the National Key Research and Development Program of China (2016YFA0600401), the National Natural Science Foundation of China (41420104002 and 41671197), the Program of Innovative Research Team of Jiangsu Higher Education Institutions of China, and the Priority Academic Program Development of Jiangsu Higher Education Institutions (164320H116). W. S acknowledges China Scholarship Council (201706860027) for the financial support. Q. Z. acknowledges support from the Swedish Research Council VR project 2017-04232 "Simulating the green Sahara with an Earth System Model." The simulations were performed on resources provided by the Swedish National Infrastructure for Computing at NSC and Cray XC30 HPC systems at ECMWF. F. S. R. P. acknowledges funding from the Swedish Research Council as part of the Joint Programming Initiative on Climate and the Belmont Forum for the project "PAlaeo-Constraints on Monsoon Evolution and Dynamics" and the financial and logistic support from the Natural Sciences and Engineering Research Council of Canada (grant RGPIN-2018-04981). This is publication number 10751 of the School of Ocean and Earth Science and Technology, publication number 1391 of the International Pacific Research Center and publication number 270 of the Earth System Modeling Center. The simulation results are available at https://pan.baidu.com/s/189yOM98SpPfRHKdPLP0p1A (Password: jx5v).

References

Adler, R. F., Huffman, G. J., Chang, A., Ferraro, R., Xie, P. P., Janowiak, J., et al. (2003). The version 2 Global Precipitation Climatology Project (GPCP) monthly precipitation analysis (1979-present). *Journal of Hydrometeorology*, *4*(6), 1147–1167. https://doi.org/10.1175/1525-7541(2003)004<1147:TVGPCP>2.0.CO;2

Bartlein, P. J., Harrison, S. P., Brewer, S., Connor, S., Davis, B. A. S., Gajewski, K., et al. (2011). Pollen-based continental climate reconstructions at 6 and 21 ka: A global synthesis. *Climate Dynamics*, *37*(3–4), 775–802. https://doi.org/10.1007/s00382-010-0904-1

Biasutti, M. (2013). Forced Sahel rainfall trends in the CMIP5 archive. *Journal of Geophysical Research: Atmospheres*, *118*, 1613–1623. https://doi.org/10.1002/jgrd.50206

Bird, B. W., Polisar, P. J., Lei, Y., Thompson, L. G., Yao, T., Finney, B. P., et al. (2014). A Tibetan lake sediment record of Holocene Indian summer monsoon variability. *Earth Planetary Science Letters*, *399*(1), 92–102. https://doi.org/10.1016/j.epsl.2014.05.017

Bonfils, C., Noblet-Ducoudre, N., Braconnot, P., & Joussaume, S. (2001). Hot desert albedo and climate change: Mid-Holocene monsoon in North Africa. *Journal of Climate*, *14*(17), 3724–3737. https://doi.org/10.1175/1520-0442(2001)014<3724:HDAACC>2.0.CO;2

Braconnot, P., Harrison, S. P., Kageyama, M., Bartlein, P. J., Masson-Delmotte, V., Abe-Ouchi, A., et al. (2012). Evaluation of climate models using palaeoclimatic data. *Nature Climate Change*, *2*(6), 417–424. https://doi.org/10.1038/nclimate1456

Braconnot, P., Harrison, S. P., Otto-Bliesner, B., Abe-Ouchi, A., Jungclaus, J., & Peterschmitt, J. Y. (2011). *The Paleoclimate Modeling Intercomparison Project contribution to CMIP5. CLIVAR Exchanges* (Vol. 16, pp. 15–19). Southampton, UK: International CLIVAR Project Office.

Davies, F. J., Renssen, H., Blaschek, M., & Muschitiello, F. (2015). The impact of Sahara desertification on Arctic cooling during the Holocene. *Climate of the Past*, *11*(3), 571–586. https://doi.org/10.5194/cp-11-571-2015

deMenocal, P., Ortiz, J., Guilderson, T., Adkins, J., Sarnthein, M., Baker, L., & Yarusinsky, M. (2000). Abrupt onset and termination of the African Humid Period: Rapid climate responses to gradual insolation forcing. *Quaternary Science Reviews*, *19*(1–5), 347–361. https://doi.org/10.1016/S0277-3791(99)00081-5

Devaraju, N., Bala, G., & Modak, A. (2015). Effects of large-scale deforestation on precipitation in the monsoon regions: Remote versus local effects. *Proceedings of the National Academy of Sciences of the United States of America*, *112*(11), 3257–3262. https://doi.org/10.1073/pnas.1423439112

Ding, Q. H., & Wang, B. (2005). Circumglobal teleconnection in the Northern Hemisphere summer. *Journal of Climate*, *18*(17), 3483–3505. https://doi.org/10.1175/JCLI3473.1

Dong, B. W., Wilcox, L. J., Highwood, E. J., & Sutton, R. T. (2019). Impacts of recent decadal changes in Asian aerosols on the East Asian summer monsoon: Roles of aerosol-radiation and aerosol-cloud interactions. *Climate Dynamics*. https://doi.org/10.1007/s00382-019-04698-0

Engelstaedter, S., Tegen, I., & Washington, R. (2006). North African dust emissions and transport. *Earth Science Reviews*, *79*(1-2), 73–100. https://doi.org/10.1016/j.earscirev.2006.06.004

Evan, A. T., Flamant, C., Gaetani, M., & Guichard, F. (2016). The past, present and future of African dust. *Nature*, *531*(7595), 493–495. https://doi.org/10.1038/nature17149

Gaetani, M., Messori, G., Zhang, Q., Flamant, C., & Pausata, F. S. R. (2017). Understanding the mechanisms behind the northward extension of the west African monsoon during the mid-Holocene. *Journal of Climate*, *30*(19), 7621–7642. https://doi.org/10.1175/JCLI-D-16-0299.1

Giannini, A., & Kaplan, A. (2018). The role of aerosols and greenhouse gases in Sahel drought and recovery. *Climatic Change*, *152*(3-4), 449–466. https://doi.org/10.1007/s10584-018-2341-9

Giannini, A., Saravanan, R., & Chang, P. (2003). Oceanic forcing of Sahel rainfall on interannual to interdecadal time scale. *Science*, *302*(5647), 1027–1030. https://doi.org/10.1126/science.1089357

Gill, A. E. (1980). Some simple solutions for heat-induced tropical circulation. *Quarterly Journal of the Royal Meteorological Society*, *106*(449), 447–462. https://doi.org/10.1002/qj.49710644905

Harrison, S. P., Bartlein, P. J., Brewer, S., Prentice, I. C., Boyd, M., Hessler, I., et al. (2014). Climate model benchmarking with glacial and mid-Holocene climates. *Climate Dynamics*, *43*(3–4), 671–688. https://doi.org/10.1007/s00382-013-1922-6

Hazeleger, W., Severijns, C., Semmler, T., Ştefănescu, S., Yang, S., Wang, X., et al. (2010). EC-Earth: A seamless Earth-system prediction approach in action. *Bulletin of the American Meteorological Society*, *91*(10), 1357–1364. https://doi.org/10.1175/2010BAMS2877.1

Hély, C., Lézine, A.-M., & Contributors, A. (2014). Holocene changes in African vegetation: Tradeoff between climate and water availability. *Climate of the Past*, *10*(2), 681–686. https://doi.org/10.5194/cp-10-681-2014

Holmes, J. A. (2008). How the Sahara became dry. *Science*, *320*(5877), 752–753. https://doi.org/10.1126/science.1158105

Hsu, P.-C., Li, T., Luo, J.-J., Murakami, H., Kitoh, A., & Zhao, M. (2012). Increasing of global monsoon area and precipitation under global warming: A robust signal? *Geophysical Research Letters*, *39*, L06701. https://doi.org/10.1029/2012GL051037

Jiang, D. B., Tian, Z. P., & Lang, X. M. (2015). Mid-Holocene global monsoon area and precipitation from PMIP simulations. *Climate Dynamics*, *44*(9-10), 2493–2512. https://doi.org/10.1007/s00382-014-2175-8

Kamae, Y., Li, X., Xie, S.-P., & Ueda, H. (2017). Atlantic effects on recent decadal trends in global monsoon. *Climate Dynamics*, *49*, 3443–3455. https://doi.org/10.1007/s00382-017-3522-3

Lau, K.-M., Ramanathan, V., Wu, G. X., Li, Z., Tsay, S. C., Hsu, C., et al. (2008). The Joint Aerosol-Monsoon Experiment: A new challenge for monsoon climate research. *Bulletin of the American Meteorological Society*, *89*(3), 369–384. https://doi.org/10.1175/BAMS-89-3-369

Lee, J.-Y., & Wang, B. (2014). Future change of global monsoon in the CMIP5. *Climate Dynamics*, *42*(1-2), 101–119. https://doi.org/10.1007/s00382-012-1564-0

Liu, J., Wang, B., Cane, M. A., Yim, S.-Y., & Lee, J.-Y. (2013). Divergent global precipitation changes induced by natural versus anthropogenic forcing. *Nature*, *493*(7434), 656–659. https://doi.org/10.1038/nature11784

Liu, J., Wang, B., Ding, Q. H., Kuang, X. Y., Soon, W., & Zorita, E. (2009). Centennial variations of the global monsoon precipitation in the last millennium: Results from ECHO-G Model. *Journal of Climate*, *22*(9), 2356–2371. https://doi.org/10.1175/2008JCLI2353.1

Madec, G. (2008). NEMO ocean engine, Note du Pole de modlisation, Institut Pierre-Simon Laplace (IPSL), Paris, France, No. 27, ISSN No. 1288–1618

McGee, D., deMenocal, P. B., Winckler, G., Stuut, J. B. W., & Bradtmiller, L. I. (2013). The magnitude, timing and abruptness of changes in North African dust deposition over the last 20,000 yr. *Earth and Planetary Science Letters*, *371-372*, 163–176. https://doi.org/10.1016/j.epsl.2013.03.054

Monerie, P.-A., Biasutti, M., & Roucou, P. (2016). On the projected increase of Sahel rainfall during the late rainy season. *International Journal of Climatology*, *36*(13), 4373–4383. https://doi.org/10.1002/joc.4638

Monerie, P.-A., Robson, J., Dong, B., Hodson, D. L. R., & Klingaman, N. P. (2019). Effect of the Atlantic multidecadal variability on the global monsoon. *Geophysical Research Letters*, *46*, 1765–1775. https://doi.org/10.1029/2018GL080903

Muschitiello, F., Zhang, Q., Sundqvist, H. S., Davies, F. J., & Renssen, H. (2015). Arctic climate response to the termination of the African Humid Period. *Quaternary Science Reviews*, *125*, 91–97, 97. https://doi.org/10.1016/j.quascirev.2015.08.012

Ning, L., Jian, L., & Sun, W. Y. (2017). Influences of volcano eruptions on Asian Summer Monsoon over the last 110 years. *Scientific Reports*, *7*(1), 42626. https://doi.org/10.1038/srep42626

Pausata, F. R., Emanuel, K. A., Chiacchio, M., Diro, G. T., Zhang, Q., Sushama, L., et al. (2017). Tropical cyclone activity enhanced by Sahara greening and reduced dust emissions during the African Humid Period. *Proceedings of the National Academy of Sciences of the United States of America*, *114*(24), 6221–6226. https://doi.org/10.1073/pnas.1619111114

Pausata, F. R., Zhang, Q., Muschitiello, F., Lu, Z., Chafik, L., Niedermeyer, E. M., et al. (2017). Greening of the Sahara suppressed ENSO activity during the mid-Holocene. *Nature Communication*, *8*(1), 16020. https://doi.org/10.1038/ncomms16020

Pausata, F. S. R., Messori, G., & Zhang, Q. (2016). Impacts of dust reduction on the northward expansion of the African monsoon during the Green Sahara period. *Earth and Planetary Science Letters*, *434*, 298–307. https://doi.org/10.1016/j.epsl.2015.11.049

Ramanathan, V., Cess, R. D., Harrison, E. F., Minnis, P., Barkstrom, B. R., Ahmad, E., & Hartmann, D. (1989). Cloud-radiative forcing and climate: Results from the earth radiation budget experiment. *Science*, *243*(4887), 57–63. https://doi.org/10.1126/science.243.4887.57

Shanahan, T. M., McKay, N. P., Hughen, K. A., Overpeck, J. T., Otto-Bliesner, B., Heil, C. W., et al. (2015). The time-transgressive termination of the African Humid Period. *Nature Geoscience*, *8*(2), 140–144. https://doi.org/10.1038/ngeo2329

Stevenson, S., Fasullo, J. T., Otto-Bliesner, B. L., Tomas, R. A., & Gao, C. C. (2017). Role of eruption season in reconciling model and proxy responses to tropical volcanism. *Proceedings of the National Academy of Sciences of the United States of America*, *114*, 1822–1826. https://doi.org/10.1073/pnas.1612505114

Sun, W. Y., Liu, J., & Wang, Z. Y. (2017). Simulation of centennial-scale drought events over eastern China during the past 1500 years. *Journal of Meteorological Research*, *31*(1), 17–27. https://doi.org/10.1007/s13351-017-6090-x

Sun, W. Y., Wang, B., Liu, J., Chen, D. L., Gao, C. C., Ning, L., & Chen, L. (2019). How northern high-latitude volcanic eruptions in different seasons affect ENSO. *Journal of Climate*, *32*(11), 3245–3262. https://doi.org/10.1175/JCLI-D-18-0290.1

Thompson, A. J., Skinner, C. B., Poulsen, C. J., & Zhu, J. (2019). Modulation of mid-Holocene African rainfall by dust aerosol direct and indirect effects. *Geophysical Research Letters*, *46*, 3917–3926. https://doi.org/10.1029/2018GL081225

Tierney, J. E., Pausata, F. S. R., & deMenocal, P. B. (2017). Rainfall regimes of the Green Sahara. *Science Advances*, *3*(1), e1601503. https://doi.org/10.1126/sciadv.1601503

Valcke, S. (2006). OASIS3 user guide, PRISM Tech. Rep. 3, 64 Partnership for Res. Infrastructures in Earth Syst. Model., Toulouse, France. Retrieved from http://www.prism.enes.org/Publications/Reports/oasis3_UserGuide_T3.pdf

Vancoppenolle, M., Fichefet, T., Goosse, H., Bouillon, S., Madec, G., & Maqueda, M. A. M. (2008). Simulating the mass balance and salinity of Arctic and Antarctic sea ice. 1. Model description and validation. *Ocean Modelling*, *27*(1–2), 33–53. https://doi.org/10.1016/j.ocemod.2008.10.005

Vecchi, G. A., Soden, B. J., Wittenberg, A. T., Held, I. M., Leetmaa, A., & Harrison, M. J. (2006). Weakening of tropical Pacific atmospheric circulation due to anthropogenic forcing. *Nature*, *441*(7089), 73–76. https://doi.org/10.1038/nature04744

Wang, B., & Ding, Q. H. (2008). Global monsoon: Dominant mode of annual variation in the tropics. *Dynamics of Atmospheres and Oceans*, *44*(3–4), 165–183. https://doi.org/10.1016/j.dynatmoce.2007.05.002

Wang, B., Lee, J.-Y., & Xiang, B. Q. (2015). Asian summer monsoon rainfall predictability: A predictable mode analysis. *Climate Dynamics*, *44*(1-2), 61–74. https://doi.org/10.1007/s00382-014-2218-1

Wang, B., Li, J., Cane, M. A., Liu, J., Webster, P. J., Xiang, B., et al. (2018). Toward predicting changes in the land monsoon rainfall a decade in advance. *Journal of Climate*, *31*(7), 2699–2714. https://doi.org/10.1175/JCLI-D-17-0521.1

Wang, B., Liu, J., Kim, H.-J., Webster, P. J., & Yim, S.-Y. (2012). Recent change of the global monsoon precipitation (1979–2008). *Climate Dynamics*, *39*(5), 1123–1135. https://doi.org/10.1007/s00382-011-1266-z

Wang, B., Liu, J., Kim, H. J., Webster, P. J., Yim, S. Y., & Xiang, B. Q. (2013). Northern Hemisphere summer monsoon intensified by mega- El Niño/southern oscillation and Atlantic multidecadal oscillation. *Proceedings of the National Academy of Sciences of the United States of America*, *110*(14), 5347–5352. https://doi.org/10.1073/pnas.1219405110

Wang, P. X., Wang, B., Cheng, H., Fasullo, J., Guo, Z. T., Kiefer, T., & Liu, Z. Y. (2014). The global monsoon across timescales: Coherent variability of regional monsoons. *Climate of the Past*, *10*(6), 2007–2052. https://doi.org/10.5194/cp-10-2007-2014

Wang, P. X., Wang, B., Cheng, H., Fasullo, J., Guo, Z. T., Kiefer, T., & Liu, Z. Y. (2017). The global monsoon across time scales: Mechanisms and outstanding issues. *Earth-Science Reviews*, *174*, 84–121. https://doi.org/10.1016/j.earscirev.2017.07.006

Zhao, Y., & Harrison, S. P. (2012). Mid-Holocene monsoons: a multi-model analysis of the inter-hemispheric differences in the responses to orbital forcing and ocean feedbacks. *Climate Dynamics*, *10*(6), 2007–2052. https://doi.org/10.5194/cp-10-2007-2014